

## Corrosion resistance of sintered duplex stainless steel evaluated by electrochemical method

L.A. Dobrzański <sup>a,\*</sup>, Z. Brytan <sup>a</sup>, M. Actis Grande <sup>b</sup>, M. Rosso <sup>b</sup>

<sup>a</sup> Division of Materials Processing Technology, Management and Computer Techniques in Materials Science, Institute of Engineering Materials and Biomaterials, Silesian University of Technology, ul. Konarskiego 18a, 44-100 Gliwice, Poland

<sup>b</sup> Materials Science and Chemical Engineering Department – Polytechnic of Torino C.so Duca degli Abruzzi, 24 10129 Torino, Italy

\* Corresponding author: E-mail address: leszek.dobrzanski@polsl.pl

Received in revised form 15.09.2006; accepted 30.09.2006

### Properties

#### ABSTRACT

**Purpose:** of this paper was to examine the corrosion resistance of duplex stainless steels using electrochemical methods in 1M NaCl solution. The influence of powder mixes preparation and cooling cycle after sintering on corrosion properties was evaluated.

**Design/methodology/approach:** In presented study duplex stainless steels were obtained through powder metallurgy starting from austenitic, martensitic base powders by controlled addition of alloying elements, such as Cr, Ni, Mo and Cu. In the studies behind the preparation of mixes, Schaeffler's diagram was taken into consideration. Prepared mixes have been compacted at 800 MPa and sintered in a vacuum furnace with argon backfilling at 1260°C for 1 h. After sintering two different cooling cycles were applied: rapid cooling with an average cooling rate of 245 °C/min and slow cooling of 5 °C/min in argon atmosphere. Produced duplex stainless steels have been studied by scanning and optical microscopy and EDS chemical analysis of microstructure components. Corrosion properties have been studied through electrochemical methods in 1M NaCl water solution

**Findings:** According to achieved results, it was affirmed that applied sintering method as well as powder mixes preparation allows for manufacturing the sintered duplex steels with good corrosion properties which depends on austenite/ferrite ratio in the microstructure and elements partitioning between phases. Corrosion resistance of sintered stainless steels is strictly connected with the density and the pore morphology present in the microstructure too. The highest resistance to pitting corrosion in 1M NaCl solution was achieved for composition with approximate balance of ferrite and austenite in the microstructure.

**Research limitations/implications:** According to the powders characteristic, the applied fast cooling rate seems to be a good compromise for corrosion properties and microstructures, nevertheless further tests should be carried out in order to examine different cooling rates.

**Originality/value:** The use of elemental powders added to a stainless steel base showed its potentialities, in terms of fair compressibility and final sintered density. In addition a good microstructural homogeneity and first of all corrosion resistance was achieved, also working with cycles possible for industries.

**Keywords:** Corrosion; Manufacturing and Processing; Powder Metallurgy; Duplex stainless steel

## 1. Introduction

Sintered stainless steels are used in many industrial branches due to their high mechanical properties and good corrosion resistance. According to profitability, high dimensional tolerance, shape reproducibility and energy saving the main receiver of parts produced by powder technology is automotive appliances industries. The powder metallurgy stainless steels, especially ferritic grades, have found applications in mounting brackets for the rear view mirrors, the tone wheels for the antilock brake systems and also in automotive exhaust applications like exhaust flanges and mounting unit of HEGOS [1-3]. The automotive market introduces newly designed sintered parts in large amounts in produced cars. Stainless steel is the preferred material for powder metal flanges because of its resistance to corrosion and oxidation. The fact that the powder metal parts can be made in high material densities for the optimum combination of properties has encouraged their use at biggest users of powder metal exhaust system flanges in the world. The usage of automobile parts manufactured by powder metallurgy is still weak in Europe [4] and Japan (Fig. 1), which is the reason of advanced researches on the sintered stainless steels especially easy to manufacture, cost effective and environmental friendly grades. Duplex stainless steels are the newest in the stainless steels family. They are characterized by a two-phase microstructure consisting of approximately equal amounts of ferrite and austenite. Duplex steels thus combine some of the features of the two major classes, austenitic and ferritic grades. Sintered duplex stainless steel seems to be very promising in those appliances what explain performed research in Europe [5÷12].

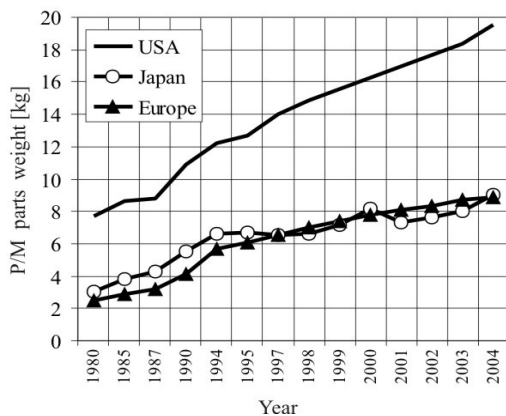


Fig. 1 Parts weight in typical vehicle made by powder metallurgy.

Pitting corrosion resistance in NaCl environment plays decisive rule in properties of stainless steels. Evaluations of electrochemical behaviour of sintered duplex steels using potentiodynamic polarization enable the determination of their properties in these conditions and make possible simulate real work conditions accelerated. In the field of powder metallurgy density highly influence the corrosion resistance due to electrolyte penetration to open porosity and corrosion proceed faster. In consequence of interconnected pores in the microstructure of sintered stainless steels, lower corrosion resistance is achieved [13-15].

This paper presents the results of researches carried out on the sintered duplex stainless steels obtained by mixing of elemental powders to an either martensitic or austenitic powder and their comparison with steel obtained trough mixing austenitic and ferritic powder in equal quantities. The work has been focused towards the evaluation of obtained microstructures and corrosion resistance in chloride containing environment.

## 2. Experimental procedure

To produce sintered duplex stainless steel different compositions have been tested, using austenitic X2CrNiMo17-12-2 (AISI 316L) and martensitic X6Cr13 (AISI 410L) (Fig. 2) as starting base water atomized powders of Hoganas Corporation with the characteristics presented in Table 1.

Table 1. Average composition of starting powders.

Grade powder	Elements concentration, wt. %								
	PN-EN	AISI	Ni	Cr	Si	Mn	Mo	C	Fe
X2CrNiMo 17-12-2	316L		13	17	0.8	0.2	2.2	0.02	bal.
X6Cr13	410L		0.14	12.2	0.88	0.09	-	0.02	bal.
X6Cr17	430L		-	16	1.14	0.19	-	0.09	bal.

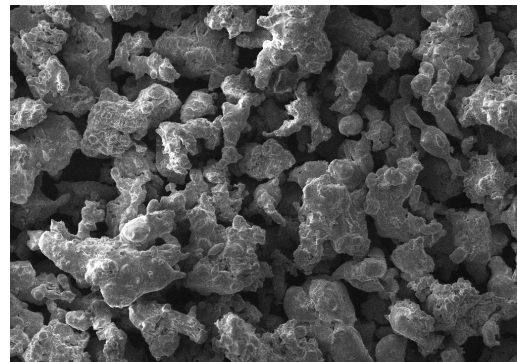


Fig. 2. The X6Cr13 stainless steel powder morphology.

Austenitic base powder X2CrNiMo 17-12-2 were mixed with addition of alloying elements powders such as Cr (in form of ferrochromium powder), Ni, Mo and Cu in the right quantity to obtain the chemical composition similar to biphasic one - mixtures A and B. Powder mixtures signed as C and D were produced starting from martensitic powder X6Cr13. Moreover, the ferritic stainless steel X6Cr17 powder has been mixed to austenitic stainless steel powder in the ratio of 1/1 in order to examine the microstructure derived after sintering (mixture E). In the preparation of powder mixtures, Schaeffler's diagram was taken into consideration (Fig. 3). Although its proper application is in welding, it is possible to extend its use in the field of powder metallurgy. Thus  $Cr_E$  and  $Ni_E$  equivalents were obtained using formulas 1 and 2 respectively.

$$Cr_E = \% Cr + \% Mo + 1.5 \cdot \% Si + 0.5 \cdot \% Nb \quad (1)$$

$$Ni_E = \% Ni + 30 \cdot \% C + 0.5 \cdot \% Mn \quad (2)$$

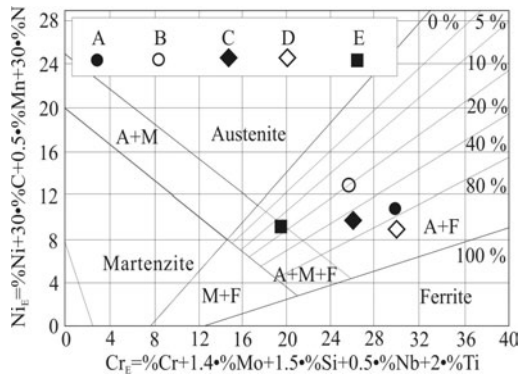


Fig. 3. Schaeffler's diagram. The marked points on the graph determine the forecast microstructure of the compositions.

The weight quantities of the corresponding elements in percent were introduced in those formulas which locate all prepared powder mixtures in a well defined area, at least from a theoretical point of view. Chemical composition of produced mixtures were placed in austenitic-ferritic area of the Schaeffler's diagram with various content of ferritic phase in the range from 20 to 80%.

Powders were mixed with single elements using a laboratory turbula mixer. Acrawax was used as lubricant in a quantity of 0.65 wt.% in excess 100 for all compositions produced. Samples were obtained using a hydraulic press applying a pressure of 800 MPa with a floating die. The debinding process was done at 550°C (823 K/min) for 60 minutes in a nitrogen atmosphere. Samples were then sintered in a vacuum furnace with argon backfilling at 1260°C (1533 K/min) for 1 h. After sintering two different cooling cycles were applied: rapid cooling with an average cooling rate of 245 °C/min (518 K/min) using nitrogen under pressure 0.6 MPa and slow cooling with furnace with an average cooling rate of 5 °C/min (278 K/min) in argon atmosphere. Table 1 presents all the prepared compositions according to Schaeffler's diagram.

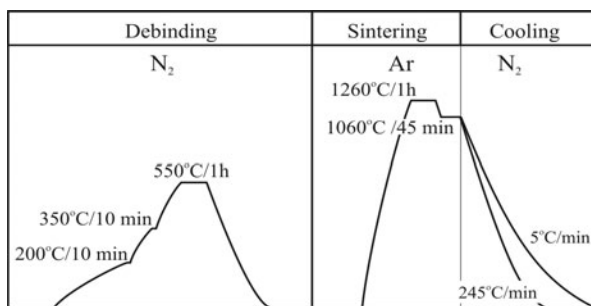


Fig. 4. Thermal cycle of debinding and sintering process

Densities were evaluated using the water displacement method. Microstructure observations were carried out using light microscope and scanning electron microscope equipped in EDS. Evaluations of the phase composition were made using ARL X'TRA 48 X-ray spectrometer, with the filtered copper lamp rays with 45kV voltage and heater current of 40mA.

Table 2. Chemical composition of investigated powder mixes.

Base powders	Composition designation	Elements concentration, wt. %						
		Ni	Cr	Si	Cu	Mn	Mo	Fe
X2CrNiMo 17-12-2	A	10.52	26.40	0.80	0.80	-	2.02	bal.
	B	11.51	21.33	0.84	2.00	-	2.21	bal.
X6Cr13	C	8.10	22.72	0.70	-	0.06	2.00	bal.
	D	8.09	26.23	0.65	2.00	0.06	2.00	bal.
X2CrNiMo 17-12-2, X6Cr17	E	6.50	16.20	1.02	0.05	0.10	1.25	bal.

Metallographic specimens of all test materials were analyzed in the unetched as well as etched conditions. Unetched metallographic samples were utilized to evaluate stereological parameters of the pore structure such as pore size and pore shape factors  $f_s$  and  $f_e$  according to formula 3 and 4. This was accomplished with a Leica Qwin image analysis system. Pore shape factor  $f_s$  determine profile irregularity of a pore while pore shape factor  $f_e$  represent the pore elongation.

$$f_s = \frac{4 \cdot \pi \cdot A}{P^2} \quad (3)$$

where A and P are the area and the perimeter, respectively, of the metallographic cross-section of the pore.

$$f_e = \frac{D_{\min}}{D_{\max}} \quad (4)$$

where,  $D_{\min}$  and  $D_{\max}$  are the minimum and the maximum Feret diameter of a pore. The shape factor of 1 represents a circular pore in the plane of analysis and as the number decreases from 1, the elongation and degree of irregularity increases.

The pitting corrosion behaviour of the sintered stainless steels was evaluated by analyzing of the polarization curves. The testing envelopment was a 1M NaCl at room temperature. The investigations were conducted using a measuring system PGP-201 with VoltaMaster 4 system. The reference electrode was a saturated calomel electrode (SCE) with platinum one used as a support electrode. The measuring procedure was started measuring the open circuit potential value and the potentiostatic curve. Next, the measuring of potentiodynamic polarization current with a scan rate 1mV/s was performed. The direction of anodic polarization was changed when the anodic current density of 10mA/cm<sup>2</sup> was achieved and then the reverse curve was measured. Corrosion rate was calculated according to 1<sup>st</sup> Stern (Tafel) method:

$$Corr.rate (\mu m / year) = \frac{i_{corr} \cdot M}{D \cdot V} \cdot 3270 \cdot 10^3 \quad (5)$$

where,  $i_{corr}$  (A/cm<sup>2</sup>) – corrosion current, M(g) – atomic mass, D(g/cm<sup>3</sup>) density, V – valence, with: 3270 = 0.01 x [1 year (in seconds) / 96497.8] and 96497.8 = 1 Faraday in Coulombs.

### 3. Results and discussion

Density results, where evaluated using the water displacement method obtained in terms of green and sintered density (Table 3). Obtained results show that for the martensitic based mixtures higher sintered densities were obtained. For the austenitic based powders, lower values were obtained, even though starting with green values similar to the other compositions. Mixture obtained by mixing ferritic and austenitic powders in equal amounts (composition E) shows good density after sintering cycle. Greater reactivity of martensitic grade powders when compared to austenitic grades results in higher shrinkage rate of the first one. Moreover, the addition of copper has resulted in the formation of a liquid phase during sintering and there through it influences on growth of sinterability caused by faster mass transport. This is evident for compositions containing copper with reason of higher sintered density when compared with sintered duplex stainless steels without copper addition.

Plot of pore shape factor  $f_s$  indicate that for all prepared mixtures his value is much the same and the major part of pores (about 50%) achieve approximately 0.75 in the case of sintering cycle with fast cooling from sintering temperature (Fig. 6). Pore shape factor  $f_e$  demonstrate major variety of pores shape and is including in the range of 0.45-0.7. There appears to be no significant change in the pore shape for all the materials that were evaluated.

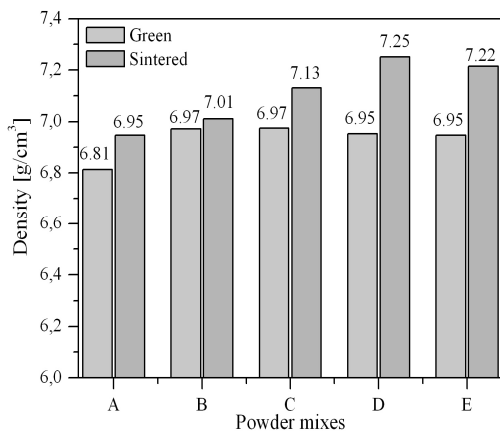


Fig. 5. Green and sintered density of studied compositions in green and as sintered state.

Table 3.

The results of green density, sintered density, total porosity and average pore size of studied compositions.

Composition designation	Theoretical density [g/cm³]	Green density [g/cm³]	Sintered density [g/cm³]	Total porosity [g/cm³]	Shrinkage [%]	Average pore area [µm²]
A	7.80	6.81	6.95	10.95	2.0	28.69
B	7.86	6.97	7.01	10.86	0.6	20.78
C	7.80	6.97	7.13	8.59	2.2	27.81
D	7.80	6.95	7.25	7.06	4.1	30.66
E	7.79	6.95	7.22	7.34	3.7	14.65

Evaluation of pore morphology in the case of sintering cycle with slow cooling after sintering indicate that pore become more spherical due to elongated temperature affect (Fig. 7). This effect is more evident for composition (E).

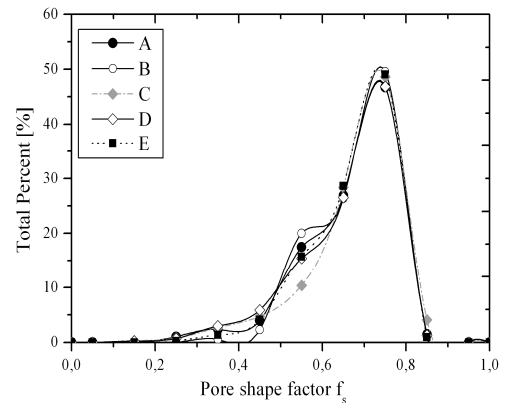


Fig. 6. Pore shape factor  $f_s$  of steels sintered and fast cooled directly from sintering temperature.

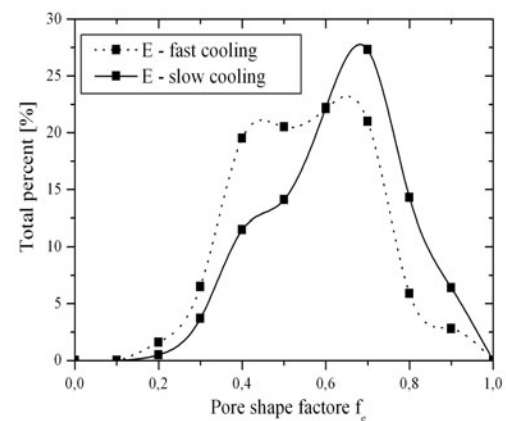


Fig. 7. Pore shape factor  $f_e$  of composition (E) cooled after sintering with different ratios.

Executed X-ray analyses confirm that the structure of the obtained sintered steels in the case of fast cooling directly from sintering temperature consists of austenite and ferrite phases.

Phase quantities in the microstructure were evaluated. Composition (A) and (D) reaches the ferrite content about 75% while composition (B) 18%. For composition (C) the approximate balance of ferrite and austenite was archived. Steel marked as (E) reach ferrite content about 67%. The obtained results prove the usefulness of the Schaeffler's diagram for predicting the types of sintered duplex stainless steels structures. Performed analyses do not demonstrate other secondary phases like sigma phase, carbides or nitrides precipitations in the microstructure of those steels. Figure 8 shows X-ray diffraction patterns of investigated sintered duplex steels with major diffractions from ferrite and austenite.

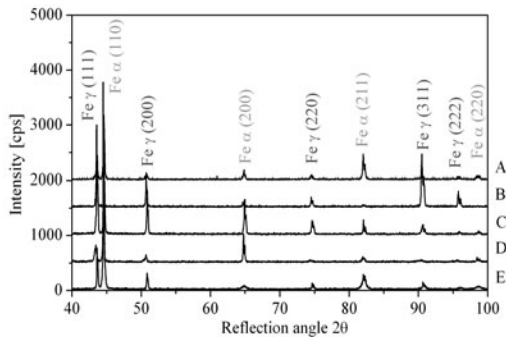


Fig. 8. X-ray diffraction patterns of sintered duplex steels.

According to metallographic examinations of obtained materials the presence of a fine microstructure with no recollection of precipitates can be seen (Fig. 9). The absence of precipitates shows that applied technology and the way of achieving mixtures result in the right microstructure. Austenite and ferrite are well mixed with an observed balancing between the two structures present throughout the sample.

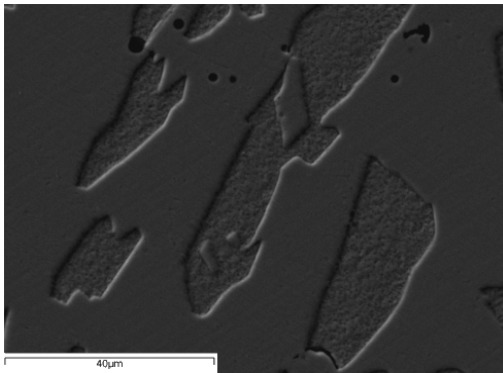


Fig. 9. Microstructure of sintered duplex stainless steel, composition (C) obtained in sintering cycle with fast cooling rate.

Chemical composition analysis (EDS) of individual structural components in studied steels shows (Fig. 10) that the concentrations of elements such as Cr and Mo in ferrite phase is higher, while Ni concentration is lower than in austenitic phase. The element partitioning between ferritic and austenitic phase is consistent with the stabilizing effect of each element on the respective phase. Concentration of alloying elements in both phases is in accordance to conventional duplex steels.

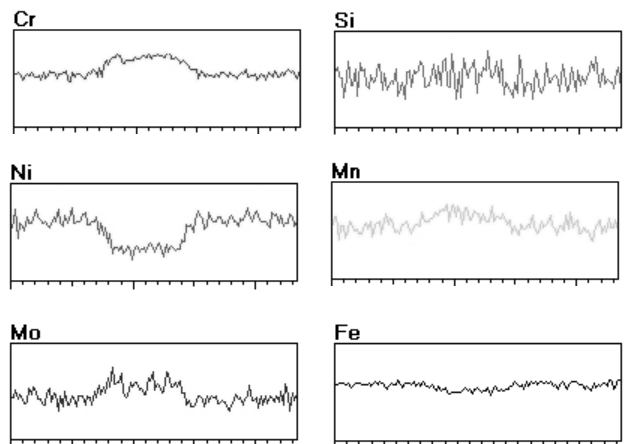
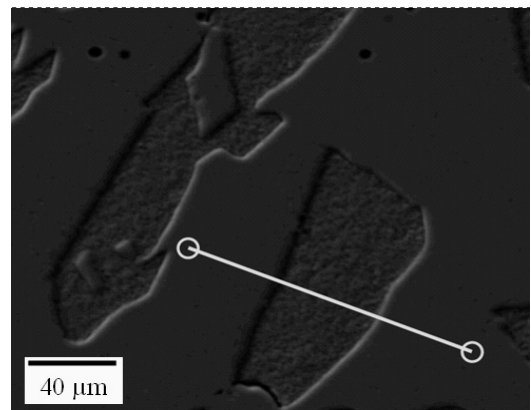


Fig. 10. Linear distribution of alloying elements performed by EDS analysis of defined ferritic grain and surrounding austenitic region in the steel (D) obtained in sintering cycle with fast cooling rate.

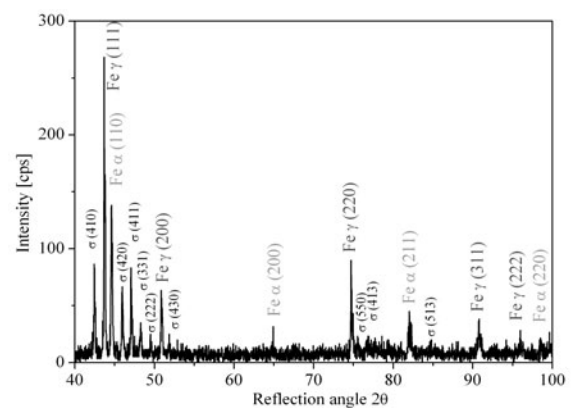


Fig. 11. X-ray diffraction pattern of sintered duplex stainless steel, composition (A) slow cooled from sintering temperature.

In the case of sintered cycle with slow cooling with furnace, precipitation of sigma phase can be seen (Figs 11, 12), except composition (E). Intermetallic sigma phase, rich in Cr and Mo precipitate on ferrite-austenite boundaries and inside ferritic grains.

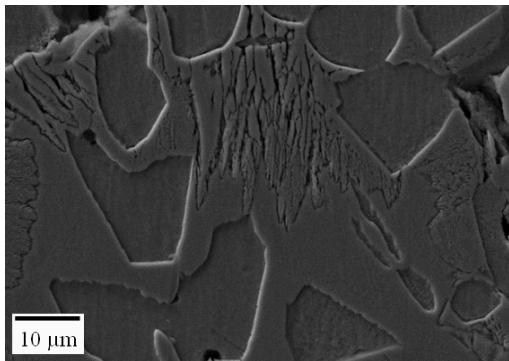


Fig. 12. Sigma phase precipitate in microstructure of composition (A) slow cooled from sintering temperature.

During cooling with slow rate, ferrites decompose on sigma phase and secondary austenite causing impoverishment of surrounded zones in alloying elements. During electrochemical tests the passivation of all analysed sintered duplex steels was not obtained and the usual active-passive transition maximum does not appear. After the passive range rapid increases of current density occur and passive layer destruction proceeds and transition to pitting corrosion region (Fig. 13, 14). The corrosion potential of sample prepared by mixing ferritic and austenitic powder in equal amounts (E) is more active and rest of the steels demonstrate lower current density in active region. In the case of composition (C) the lowest increase of current density in active region was found. Moreover the lowest corrosion current density value was found for (C) composition. It is remarkable to notice a limit current density of about 12mA/cm<sup>2</sup> was measured for this composition while for (E) about 22mA/cm<sup>2</sup> (Fig. 15, 16).

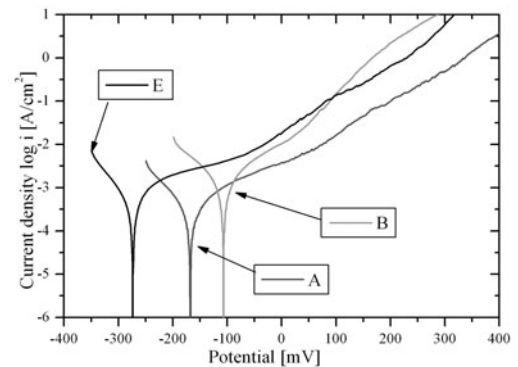


Fig. 13. Potentiodynamic curves of analysed sintered duplex stainless steels in 1M NaCl obtained in sintering cycle: 1260°C, 60min, rapid cooling after sintering, compositions A, B and E.

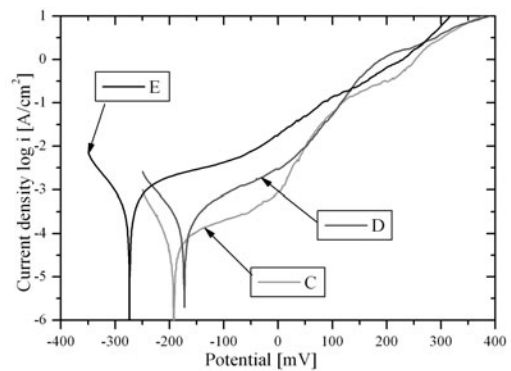


Fig. 14. Potentiodynamic curves of analysed sintered duplex stainless steels in 1M NaCl obtained in sintering cycle: 1260°C, 60min, rapid cooling after sintering, compositions C, D and E.

Table 4. The potentiodynamic polarization results in 1M NaCl.

Composition designation	Cooling after sintering	$E_{corr}$ [mV]	$i_{corr}$ [ $\mu$ A/cm <sup>2</sup> ]	$R_p$ [k $\Omega$ /cm <sup>2</sup> ]	$E_{br}$ [mV]	Corrosion rate [ $\mu$ m/Y]
A	fast	-163,97	0,22	74,74	330	2,78
	slow	-90,9	0,73	32,73	305	9,39
B	fast	-99,80	1,35	14,70	170	17,23
	slow	-62,6	2,74	11,13	310	34,84
C	fast	-188,85	0,06	254,40	240	0,81
	slow	-287,35	0,008	311,71	230	0,148
D	fast	-151,15	0,13	93,15	270	1,71
	slow	-180,26	0,042	143,18	190	0,543
E	fast	-273,55	0,37	36,66	260	4,71
	slow	-274,6	0,4322	31,97	255	5,53

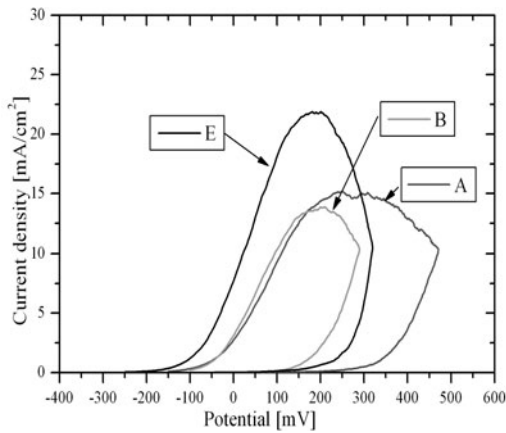


Fig. 15. Potentiodynamic curves of analysed sintered duplex stainless steels in 1M NaCl obtained in sintering cycle: 1260°C, 60min, rapid cooling after sintering, compositions A, B and E.

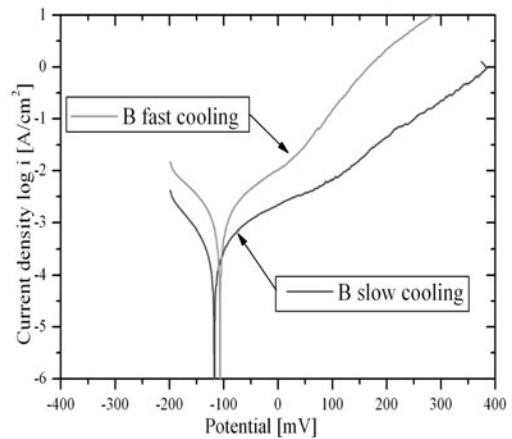


Fig. 18. Comparison of potentiodynamic curves of composition B sintered in different cycles.

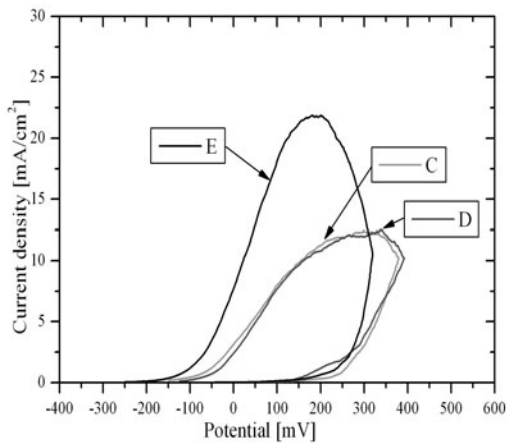


Fig. 16. Potentiodynamic curves of analysed sintered duplex stainless steels in 1M NaCl obtained in sintering cycle: 1260°C, 60min, rapid cooling after sintering, compositions C, D and E.

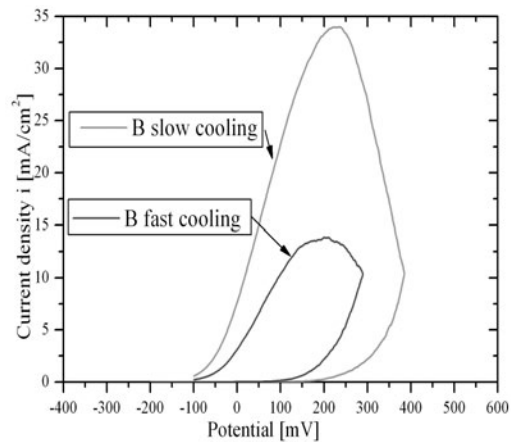


Fig. 19. Comparison of potentiodynamic curves of composition B sintered in different cycles.

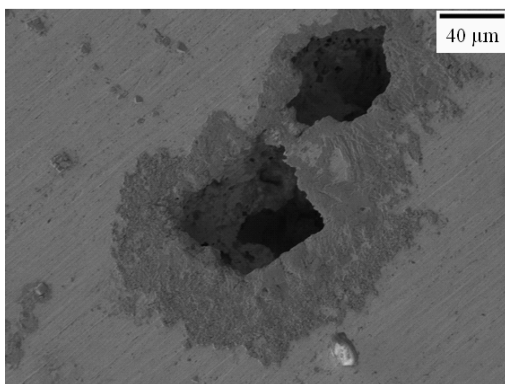


Fig. 17. Corrosive pits in microstructure of sintered duplex stainless steel – composition (C) fast cooled after sintering cycle.

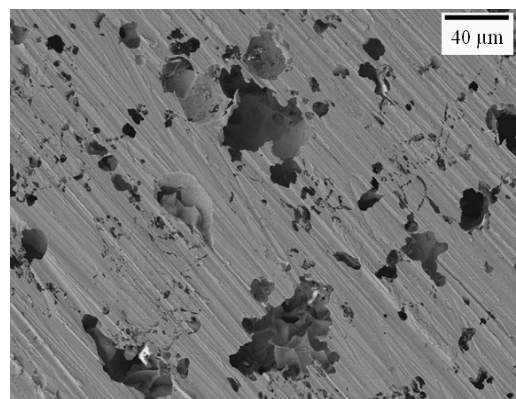


Fig. 20. Corrosive pits in microstructure of sintered duplex stainless steel – composition (C) slow cooled after sintering cycle.

The main results deriving from performed electrochemical test is repeatedly higher corrosion resistance of produced balanced ferritic-austenitic microstructure compared to other composition (Tab. 4). The pitting resistance of martensitic base powder compositions is higher when compared to austenitic base powder compositions even when the chemical composition is taken into consideration.

The corrosive pits initially are formed in open porosity (Fig. 17, 20) and then proceed into interior of the pore – this mechanism is valid for all analyzed sintered steels.

Sintering and slow cooling with furnace result in the sigma phase precipitations in microstructure of analyzed steels. This effect is evident in case of compositions based on austenitic base powder and especially for composition B (Fig. 18, 19). Compositions based on martensitic powder C and D exhibit increase of corrosion resistance when cooled slow, what can be the reason of elongated time exposure thus provoking pore rounding.

## 4. Conclusions

According to achieved results, duplex stainless steels can be obtained starting from stainless steels powders (austenitic, ferritic and martensitic) by simple addition of single elements, through a common industrial process in vacuum. Manufactured steels demonstrate the austenitic - ferritic structure with regular arrangement of both phases with no presents of precipitates in case of rapid cooling after sintering. The microstructure of sintered duplex steel basing on X2CrNiMo17-12-2 (AISI 316L) and XCr17 (AISI 430L) base powders mixed in equal content is more coarse-grained when compared to steels obtained by addition of elemental powders to martensitic base powder XCr13 (AISI 410L), where ferritic and austenitic grains are fine and well mixed.

According to corrosion test results newly developed sintered duplex steels are characterized by good corrosion resistance to 1M NaCl solution. Corrosion resistance of sintered stainless steels is strictly connected with the density and the pore morphology present in the microstructure too. The highest resistance to pitting corrosion in 1M NaCl solution was achieved for composition with approximate balance of ferrite and austenite in the microstructure and additionally the better results was obtained for compositions based on martensitic powders due to highest density witch highly influence on corrosion properties.

The main disadvantage of use of the sintered duplex stainless steels, compared to similar wrought materials is the lower corrosion resistance. Solution of this situation can be production of large number of parts with complex geometry and small size by powder metallurgy. So, the use of those steels in automobile appliances industry could be possible and cost-effective.

## Acknowledgements

Investigations were partially financed within the framework of the Polish State Committee for Scientific Research grant No 3T08A 078 29/2005 headed by Prof. L.A. Dobrzański.

## References

- [1] P.K. Samal, J. B. Terrell, Mechanical properties improvement of PM 400 series stainless steels via nickel addition, *Metal Powder Report* December (2001) 28-34.
- [2] A. J. Rawlings, H. M. Kopech, H. G. Rutz, The effect of service temperature on the properties of ferritic P/M stainless steels, *Proceedings of International Conference on Powder Metallurgy & Particulate Materials PM2TEC'97*, Chicago USA, 1997.
- [3] W. Brian James, What is sinter-hardening?, *Proceedings of International Conference on Powder Metallurgy & Particulate Materials PM2TEC'98*, Las Vegas, Nevada USA, 1998.
- [4] D. Schaefer, C.J. Trombino, State of North American P/M industry 2005, *PM2TEC'2005*, Montreal, Canada.
- [5] L.A. Dobrzański, Z. Brytan, M. Actis Grande, M. Rosso, E. J. Pallavicini, Properties of vacuum sintered Duplex Stainless Steels, *Journal of Materials Processing Technology*, Vol. 157-158 (2004) 312-316.
- [6] M. Campos, A. Bautista, D. Caceres, J. Abenojar, J.M. Torralba, Study of the interfaces between austenite and ferrite grains in P/M duplex stainless steels, *Journal of the European Ceramic Society* Vol. 23 (2003) 2813-2819.
- [7] P. Datta, G.S. Upadhyaya, Sintered duplex stainless steels from premixes of 316L and 434L powders, *Materials Chemistry and Physics* Vol. 67 (2001) 234-242.
- [8] L.A. Dobrzański, Z. Brytan, M. Actis Grande, M. Rosso., *Struktura i własności spiekanych stali typu duplex*, *Proceedings of 12<sup>th</sup> International Scientific Conference AMME'03*, pp.211-214, Gliwice-Zakopane, Poland 2003.
- [9] M. Actis Grande, D. Ugues, M. Rosso, L.A. Dobrzański, Z. Brytan, The PM route for duplex stainless steels, *Proceedings of 12<sup>th</sup> International Scientific Conference AMME'03*, Gliwice-Zakopane, Poland 2003, 5-8.
- [10] M. Actis Grande, D. Ugues, L.A. Dobrzański, Z. Brytan, M. Rosso, Properties of vacuum sintered duplex stainless steels, *Proceedings of Powder Metallurgy World Congress & Exhibition PM2004*, Vienna, Austria Vol. 3, 2004, 395-399.
- [11] J. Kazior, T. Pieczonka, A. Molinari, Properties of AISI 316L, AISI 434L and duplex stainless steel, *Proceedings of 8<sup>th</sup> International Scientific Conference AMME'1999*, Gliwice, 1999, 289-292.
- [12] M. Campos, P. Sarasola, J.M. Torralba, Sintering evolution of duplex stainless steels obtained from austenitic and ferritic stainless steels powders mixtures, *Proceedings of 9<sup>th</sup> International Scientific Conference AMME'2000*, Gliwice – Sopot – Gdańsk, Poland, 2000, 83-86.
- [13] D.Y. Kobayashi, S. Wolyneć, Evaluation of the Low Corrosion Resistant Phase Formed During the Sigma Phase Precipitation in Duplex Stainless Steels, *Materials Research*, Vol. 2, No. 4, 1999, 239-247.
- [14] R.A. Perren, T. Suter, C. Solenthaler, G. Gullo, P.L. Uggowitzer, H. Böhni, M.O. Speidel, Corrosion resistance of super duplex stainless steels in chloride ion containing environments: investigations by means of a new microelectrochemical method II. Influence of precipitates, *Corrosion Science*, 43 (2001) 727-730.
- [15] L.A. Dobrzański, Z. Brytan, M. Actis Grande, M. Rosso, Corrosion resistance of sintered duplex stainless steel evaluated by electrochemical method, *Worldwide Journal of Achievements in Materials and Manufacturing*, vol 17, (2006) 317-320.